Phenomenology of a 750 GeV singlet

Adam Falkowski,[a] **Oren Slone**[b] **and Tomer Volansky**[b]

[a]*Laboratoire de Physique Théorique, Bat. 210, Université Paris-Sud,*
91405 Orsay, France

[b]*Raymond and Beverly Sackler School of Physics and Astronomy, Tel-Aviv University,*
Tel-Aviv 69978, Israel

E-mail: adam.falkowski@th.u-psud.fr, shtangas@gmail.com,
tomerv@post.tau.ac.il

ABSTRACT: We study the recently reported excess in the diphoton resonance search by ATLAS and CMS. We investigate the available parameter space in the combined run-1 and run-2 diphoton data and study its interpretation in terms of a singlet scalar field which possibly mixes with the Standard Model Higgs boson. We show that the mixing angle is already strongly constrained by high-mass Higgs searches in the diboson channel, and by Higgs coupling measurements. While a broad resonance is slightly favored, we argue that the signal is consistent with a narrow-width singlet which couples to colored and electromagnetically-charged vector-like fermions. Dijet signals are predicted and may be visible in upcoming analyses. Allowing for additional decay modes could explain a broader resonance, however, we show that monojet searches disfavor a large invisible width. Finally, we comment on the possible relation of this scenario to the naturalness problem.

Contents

1   Introduction

The analyses of proton-proton collisions at the center-of-mass energy $\sqrt{s} = 13\,\mathrm{TeV}$ at the LHC reveal an excess in the diphoton spectrum near the invariant mass $m_{\gamma\gamma} = 750\,\mathrm{GeV}$ [1, 2]. If confirmed by next year's LHC data or observed in related channels, this will mark a long-overdue discovery of physics beyond the Standard Model (SM). The simplest explanation of such a signal is a new boson with $m \simeq 750\,\mathrm{GeV}$ decaying into 2 photons, which, according to the Landau-Yang theorem [3, 4], must have spin zero, two, or higher. The origin of this resonance, and its possible interactions with the SM are a priori only mildly constrained.

In this paper we discuss theoretical interpretations of the excess, focusing on the spin-0 case. Indeed, new scalars with $\mathcal{O}(100)\,\mathrm{GeV}$-$\mathcal{O}(1)\,\mathrm{TeV}$ masses are highly motivated by the fine-tuning problem of the SM. Most theories addressing the naturalness problem predict an extended Higgs sector, for example the 2nd Higgs doublet in the MSSM, the radial Higgs boson in the twin Higgs model [5], or the radion in the Randall-Sundrum model [6]. Furthermore, new scalars in this mass range are predicted by Higgs portal dark matter models [7] or more general scenarios with hidden sectors [8], where they act as mediators between the SM and the hidden sectors. The crucial point is that for new CP-even scalars it is very natural (and in many case inevitable) to mix with the SM Higgs boson. Typically, the mixing angle is expected to be $\mathcal{O}(m_h^2/m_S^2) \approx 0.01$-$0.1$. As a consequence, the singlet would acquire the Higgs-like couplings to the SM matter, and the Higgs boson couplings would be reduced compared to the SM value (see e.g. [9] for a discussion of the Higgs phenomenology). It is important to understand the phenomenological consequences of the mixing and experimental constraints on the mixing angle when the new scalar is responsible for the 750 GeV excess.

To this end, we first introduce a trivial toy model, where a singlet scalar S couples to a new vector-like quark that carries SM color and electric charges. After integrating out the vector-like quarks at one loop, the singlet acquires an effective coupling to photons and gluons. Thanks to that coupling, the scalar can be produced at the LHC via gluon-gluon collisions, and it can decay into two photons, much like the SM Higgs boson. We show that one can find the parameter space where the observed 750 GeV excess in ATLAS and CMS can be explained. Moreover, the interesting parameter space is not completely excluded by run-1 searches. This toy model is a simple existence proof, and it can serve as a building block of more sophisticated constructions.

Subsequently, we study the feasibility of the scenario where a singlet 750 GeV scalar mixes with the Higgs doublet. We show that the mixing angle is already strongly constrained by high-mass Higgs searches in the diboson channel, and by Higgs coupling measurements. Mixing angles larger than $\sin \alpha \sim 0.1$ are impossible to achieve in this framework. This puts a strong constraint on any scenario where the new scalar is somehow involved in electroweak symmetry breaking.

We also briefly comment on the issue of naturalness. While the full discussion strongly depends on the complete model in which the new scalar is embedded, we point out that the new scalar may be relevant for this issue. Namely, in the parameter space favored by the excess it is possible that the new scalar and the vector-like quarks take part in cancellation of quadratic divergences of the Higgs boson.

The paper is organized as follows. In section 2, we study the ATLAS and CMS diphoton data, identifying the best fit mass, cross-section and width of the proposed scalar. In section 3 we introduce a minimal toy model which explains the excess via an effective field theory of a singlet that couples to gluons and photons. The basic features of the model and viable parameter space are identified. The toy-model is then extended in section 4, where we allow the singlet to mix with the SM Higgs. In section 5 we briefly discuss the implications of a broad resonance followed by the possible constraints and predictions in section 6. We conclude in section 7 with a discussion of the possible connection with the naturalness problem. While this work was in progress, these studies were published [10–27]. A number of them present ideas that have some overlap with our study.

2   A new resonance?

The ATLAS experiment presented the diphoton spectrum measured with 3.2 fb^{-1} collected at $\sqrt{s} = 13$ TeV [1]. In the bins around 750 GeV, the ATLAS experiment reports the following number of observed events and the estimated SM background prediction:

Bin[GeV]	650	690	730	770	810	850
N_{events}	10	10	14	9	5	2
$N_{\text{background}}$	11.0	8.2	6.3	5.0	3.9	3.1

The largest excess is in the bins centered at 730 and 770 GeV. The local significance of the excess at 750 GeV is quoted by ATLAS as 3.6 σ. There is no evidence for unusual
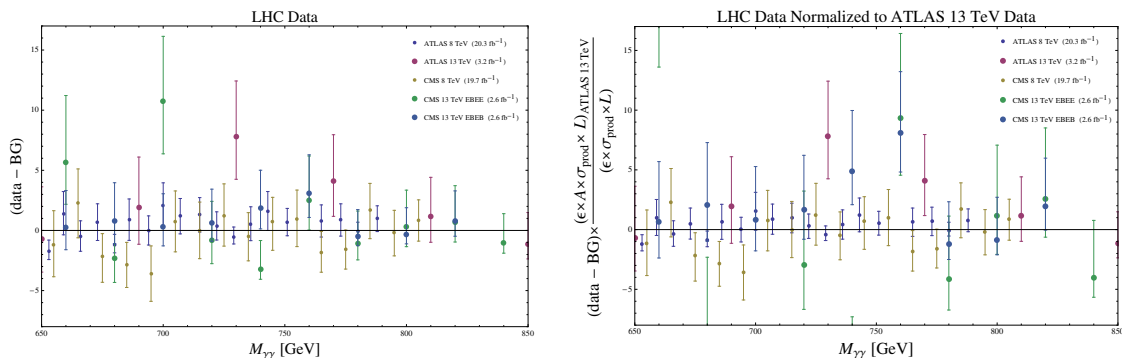
Figure 1. All data sets collected by both the ATLAS and CMS experiments at $\sqrt{s} = 8\,\text{TeV}$ and $\sqrt{s} = 13\,\text{TeV}$ runs. The points correspond to the number of events observed in each bin minus the background fitted functions for each dataset. *Left:* number of events minus background reported by each analysis. *Right:* the same data normalized to the ATLAS 13 TeV cross section, luminosity, acceptance and efficiency. The error bars are normalized as the square root of the data normalization.

additional activity (jets, missing energy) in the diphoton events in the excess region, which puts constraints on the production mode of the hypothetical resonance.

CMS uses 2.6 fb^{-1} collected at $\sqrt{s} = 13\,\text{TeV}$, and their results are given separately for 2 distinct diphoton categories. In the first category (EBEB) both photons are detected in the barrel, whereas in the second (EBEE) one photon is detected in the barrel and the other is found in the end cap. The efficiency and acceptance for potential new resonance signals are significantly different in the two categories. In the bins around 750 GeV they find [2]:

Bin[GeV]	700	720	740	760	780	800
N_{events} (EBEB)	3	3	4	5	1	1
$N_{\text{background}}$ (EBEB)	2.7	2.5	2.1	1.9	1.6	1.5
N_{events} (EBEE)	16	4	1	6	2	3
$N_{\text{background}}$ (EBEE)	5.2	4.6	4.0	3.5	3.1	2.8

The EBEB category has a mild excess in the two bins centered at 740 and 760 GeV, which coincides with the ATLAS excess. The EBEE category (a priori less sensitive) has a very large excess at 700 GeV, however without matching signals in the other more sensitive CMS category or in the ATLAS data. The local significance of the excess reported by CMS is 2.6 σ at around 750 GeV.

Figure 1 (left) shows the reported data minus background from both experiments at $\sqrt{s} = 8$ and 13 TeV [1, 2, 28, 29]. Figure 1 (right) presents the same data normalized to the ATLAS 13 TeV cross section, luminosity, acceptance and efficiency. The normalized CMS 13 TeV data exhibits better correspondence to the ATLAS 13 TeV data at around 750 GeV. Both the ATLAS and CMS 8 TeV normalized data sets show a mild excess at around 750 GeV.

In what follows we interpret the reported results in the context of a simple extension of the SM. We take a simplified model which includes one additional real scalar, S, which
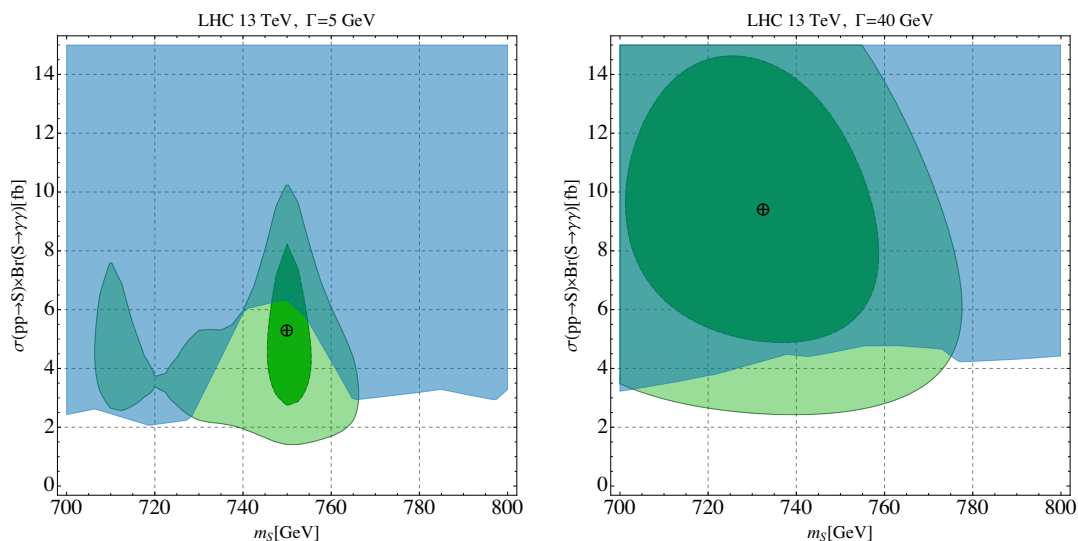
Figure 2. The 68% CL (darker green) and 95% CL (lighter green) regions in the plane of mass vs. cross-section of a scalar resonance decaying to 2 photons favored by the ATLAS and CMS run-2 data . The results are presented assuming a Breit-Wigner shape with $\Gamma_S = 5\,\text{GeV}$ *(left)* and $\Gamma_S = 40\,\text{GeV}$ *(right)*. The blue area is the region excluded by the CMS narrow (left) and wide (right) scalar resonance search in run-1 [29].

has an effective coupling to photons and gluons. In sections 3–4 we discuss possible models in more detail. To interpret the above excess we incorporate four distinct data sets. For ATLAS we use the diphoton search at $\sqrt{s} = 8\,\text{TeV}$ [28] using $20.3\,\text{fb}^{-1}$ of data, and the $\sqrt{s} = 13\,\text{TeV}$ [1] search with $3.2\,\text{fb}^{-1}$ discussed above. For CMS we take the diphoton searches at $\sqrt{s} = 8$ [29] using $19.7\,\text{fb}^{-1}$ and the 13 TeV search [2] with $2.6\,\text{fb}^{-1}$.

We work under the assumption that the new particle is dominantly produced via gluon fusion. We mimic a resonant signal using the Breit-Wigner distribution for the scalar mass $m_S \in [700 - 800]$ GeV and the width $\Gamma_S \in [5, 100]\,\text{GeV}$. We then perform a Poissonian likelihood analysis in order to find the best fit to the data as a function of three free parameters: (i) the singlet mass, m_S, (ii) its width, Γ_S, and (iii) production times branching ratio rate, $\sigma(pp \to S) \times \text{Br}(S \to \gamma\gamma)$. The production cross section times branching fraction is scaled by efficiency factors for each analysis.[1] This procedure is applied to the following combined data sets:

1. ATLAS 13 TeV + CMS 13 (LHC 13 TeV)

2. ATLAS 8 and 13 TeV + CMS 8 and 13 TeV (LHC 8 and 13 TeV).

The results are presented in the m_S vs $\sigma(pp \to S) \times \text{Br}(S \to \gamma\gamma)$ plane for two values of $\Gamma_S = 5\,\text{GeV}$ (of the order of the the experimental resolution) and $\Gamma_S = 40\,\text{GeV}$ (equal to

---

[1]For the $\sqrt{s} = 13\,\text{TeV}$ diphoton analyses, we calculated the efficiency times acceptance for a scalar resonance produced via gluon fusion using Monte Carlo simulated data. For the ATLAS search we find $\epsilon \times A \approx 0.65$ at $M_{\gamma\gamma} = 750\,\text{GeV}$. For the CMS search we find $\epsilon \times A \approx 0.48(0.21)$ for the EBEB (EBEE) category at $M_{\gamma\gamma} = 750\,\text{GeV}$. For the 8 TeV diphoton analyses we use the efficiency times acceptance quoted by refs. [28, 29].
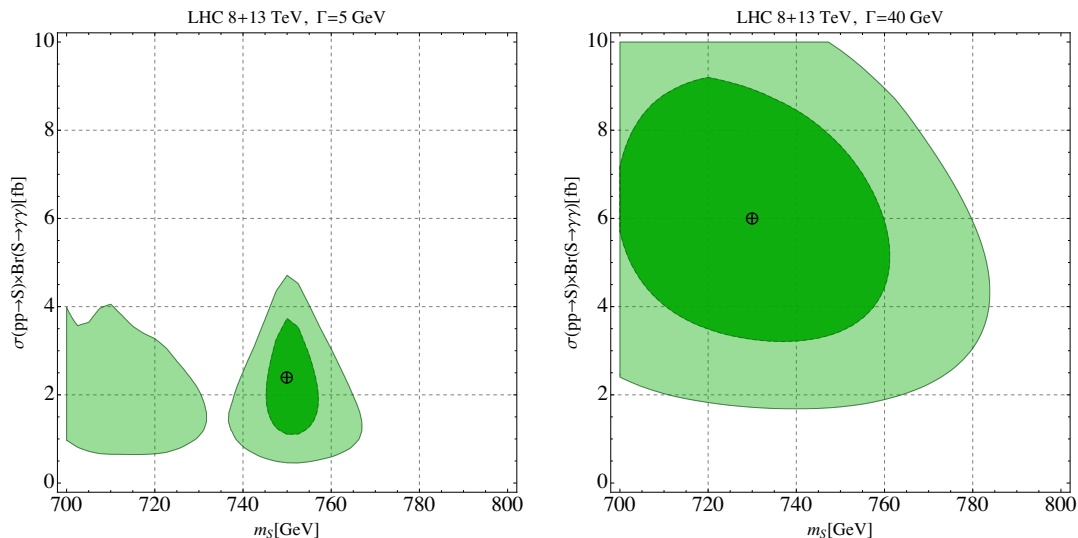
Figure 3. The 68% CL (darker green) and 95% CL (lighter green) regions in the plane of mass vs. cross-section of a scalar resonance decaying to 2 photons favored by the ATLAS and CMS run-1 and run-2 data. The results are presented assuming a Breit-Wigner shape with $\Gamma = 5\,\text{GeV}$ (left) and $\Gamma = 40\,\text{GeV}$ (right).

the bin width in [1]). The green colored regions indicate the regions of the parameter space with 68% and 95% CL favored by the data. Figures 2 and 3 present results for data sets (1) and (2) respectively. The values of mass and cross section times BR with the highest likelihood for each data set considered are:

	m_S	$\sigma(pp \to S) \times \text{Br}(S \to \gamma\gamma)$
LHC 13 TeV, $\Gamma = 5\,\text{GeV}$	$\sim 750\,\text{GeV}$	$\sim 5.3\,\text{fb}$
LHC 13 TeV, $\Gamma = 40\,\text{GeV}$	$\sim 730\,\text{GeV}$	$\sim 9.4\,\text{fb}$
LHC 8 and 13 TeV, $\Gamma = 5\,\text{GeV}$	$\sim 750\,\text{GeV}$	$\sim 2.4\,\text{fb}$
LHC 8 and 13 TeV, $\Gamma = 40\,\text{GeV}$	$\sim 730\,\text{GeV}$	$\sim 6.0\,\text{fb}$

If the 13 TeV data only are used, a narrow width resonance with 750 GeV mass and 6 fb cross section provides a very good fit to the data. There is some tension with the run-1 data, however the best fit point is not excluded by the previous diphoton analysis. We do not find any preference for a large width in the combined ATLAS and CMS data: actually, the best fit points for $\Gamma_S = 5\,\text{GeV}$ has χ^2 smaller by one unit than the one for $\Gamma_S = 40\,\text{GeV}$. Once we combine 8 and 13 TeV data, the best fit point moves to a smaller cross section, however the statistical significance of the excess remains high: $\Delta\chi^2 \approx 13$ compared to the SM point for $\Gamma_S = 40\,\text{GeV}$. In the combined run-1 and run-2 data a resonance width larger than the experimental resolution is slightly preferred.

In figure 4 we also show the best fit region for $m_S = 750\,\text{GeV}$ in the plane of the resonance width vs cross section. We see slight preference for a large width: the best fit point occurs for $\Gamma_S = 30\,\text{GeV}$, and $\sigma = 4.8\,\text{fb}$. Finally, in the full 3D scan we find the best
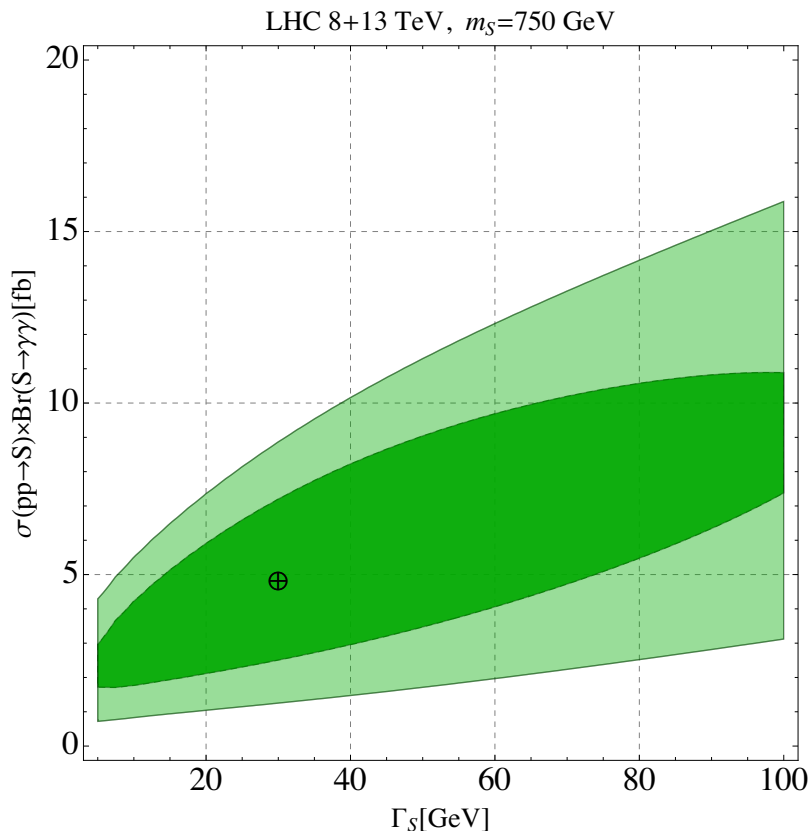
Figure 4. The 68% CL (darker green) and 95% CL (lighter green) regions in the plane of width vs. cross-section of a 750 GeV scalar resonance decaying to 2 photons favored by the ATLAS and CMS run-1 and run-2 data.

fit point for $m_S \approx 730\,\mathrm{GeV}$, $\sigma \approx 6\,\mathrm{fb}$, and $\Gamma_S \approx 40\,\mathrm{GeV}$. This is preferred over the best fit point with $\Gamma_S = 5\,\mathrm{GeV}$ by $\Delta\chi^2 \approx 2.5$.

3 Toy model: a singlet

We begin by studying a minimal model which addresses the excess discussed above. We introduce a real scalar, S, coupled to photons and gluons

$$\mathcal{L}_{S,\mathrm{eff}} = \frac{e^2}{4v}c_{s\gamma\gamma}SA_{\mu\nu}A_{\mu\nu} + \frac{g_s^2}{4v}c_{sgg}SG_{\mu\nu}^a G_{\mu\nu}^a, \tag{3.1}$$

where e is the electromagnetic constant, g_s is the QCD coupling constant, and $v \simeq 246\,\mathrm{GeV}$ is introduced for dimensional reasons. In our numerical analyses we use the SM couplings evaluated at 750 GeV, $g_s = 1.07$, and $e = 0.31$. These couplings are non-renormalizable, but they may arise effectively in a renormalizable model after integrating out vector-like quarks at one loop. We assume the singlet has a Yukawa coupling y_X to a vector-like quark X which resides in the fundamental representation of $\mathrm{SU}(3)_c$ and has mass m_X and electric charge Q_X,

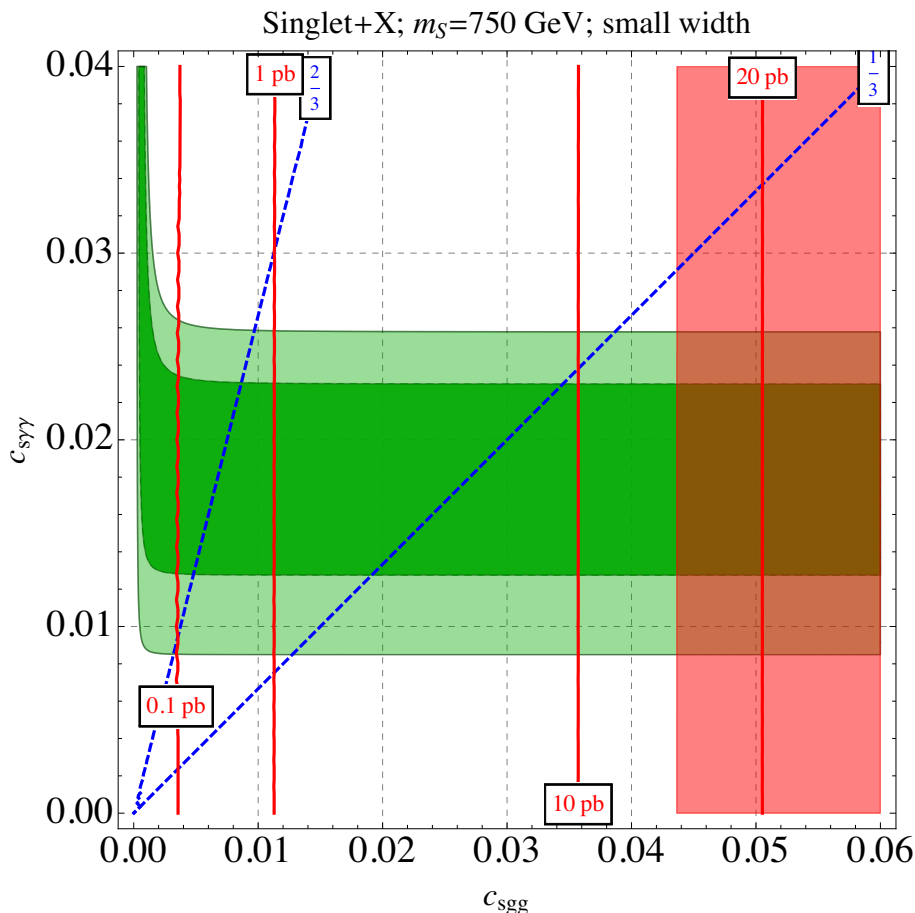$$\mathcal{L} \supset -y_X S\bar{X}X \,. \tag{3.2}$$

Figure 5. The 68% CL (darker green) and 95% CL (lighter green) regions of the parameter space favored by the ATLAS and CMS diphoton data from run-1 and run-2, assuming a singlet with $m_S = 750$ GeV. The blue lines correspond to the couplings generated from integrating out a vector-like quark with $Q_X = 2/3$ (leftmost) and $Q_X = 1/3$ (rightmost) interacting via a Yukawa coupling with the singlet. The red lines are contours of constant $\sigma(pp \to gg)$ cross section at $\sqrt{s} = 13$ TeV LHC. The red-shaded area is excluded by the CMS dijet resonance search at $\sqrt{s} = 8$ TeV [34].

Assuming $m_X \gtrsim m_S$, we integrate out X to generate the following effective couplings to gluons and photons (see e.g. [30–33]):

$$c_{sgg} = \frac{y_X v}{12\pi^2 m_X}\,, \qquad c_{s\gamma\gamma} = \frac{y_X Q_X^2 v}{2\pi^2 m_X}\,. \tag{3.3}$$

As a consequence, the ratio between the photon and gluon couplings is fixed by the electric charge of X, $c_{s\gamma\gamma} = 6Q_X^2 c_{sgg}$.

The partial decay widths mediated by these effective couplings are given by,

$$\Gamma(S \to \gamma\gamma) = c_{s\gamma\gamma}^2 \frac{e^4 m_S^3}{64\pi v^2}\,, \qquad \Gamma(S \to gg) = c_{sgg}^2 \frac{g_s^4 m_S^3}{8\pi v^2}\,. \tag{3.4}$$

Assuming that S can decay only to gluons and to photons, the branching fraction for the

photon decays is found to be,

$$\mathrm{Br}(S \to \gamma\gamma) = \frac{e^4 c_{s\gamma\gamma}^2}{8 g_s^4 c_{sgg}^2 + e^4 c_{s\gamma\gamma}^2} \,. \tag{3.5}$$

Under the same assumption, the total decay width of S is always small for perturbative values of y_X and $m_X \gtrsim 1\,\mathrm{TeV}$. In the narrow width approximation, the tree-level production cross section of the scalar is given by:

$$\sigma(pp \to S) = k \frac{\pi c_{sgg}^2 g_s^4 m_S^2}{64 v^2 E_{\mathrm{LHC}}^2} L_{gg}\left(\frac{m_S^2}{E_{\mathrm{LHC}}^2}\right), \tag{3.6}$$

where L_{gg} is the gluon luminosity function, and the k-factor accounts for the higher-order QCD corrections. The gluon luminosity is obtained using the central value of the NNLO MSTW2008 PDFs [35]. With this choice, matching to the known NNLO cross sections of a Higgs-like scalar [36], we estimate $k \approx 3.4$.

With the above, we are now ready to estimate the range of parameters of the toy model that fit the ATLAS and CMS excess, fixing its mass, $m_S = 750\,\mathrm{GeV}$ and assuming a narrow width. The results are shown in figure 5. The best fit regions are obtained assuming $m_S = 750\,\mathrm{GeV}$ contributing to two ATLAS bins at 730 and 770 GeV, and to two CMS bins at 740 and 760 GeV. In the entire displayed region $\Gamma_S \lesssim 1\,\mathrm{GeV}$, which a posteriori justifies the use of narrow width approximation.

The experimentally favored region corresponds to the effective coupling to photons in the range $c_{s\gamma\gamma} \in [0.02, 0.04]$, and the couplings to gluon $c_{sgg} \gtrsim 0.01$. Clearly, large Yukawa couplings are needed to arrive at the effective couplings in that ballpark. For example, for a vector-like top quark X with $Q_X = 2/3$, $m_X = 1\,\mathrm{TeV}$, and $y_X = 5$ one finds $c_{sgg} \simeq 0.01$, $c_{s\gamma\gamma} \simeq 0.03$. Alternatively, one can employ several vector-like quarks with smaller Yukawa couplings.

In figure 5 we also display the contours of the digluon production cross section at $\sqrt{s} = 13\,\mathrm{TeV}$, which varies between $\mathcal{O}(0.1)$ pb and $\mathcal{O}(10)$ pb in the interesting parameter space. Note that the current run-2 LHC dijet resonance searches [37, 38] do not probe the region at 750 GeV at all. We stress that it is this dijet signal in the above cross-section range that is the cleanest model-independent verification of this scalar interpretation of the resonance. The upcoming ATLAS trigger-level dijet analysis may therefore shed light on this interpretation. The dijet cross-section in run-1 is predicted to be a factor of ~ 5 smaller. Except for a very large c_{sgg}, this is not excluded by the existing run-1 analyses, which set the limit $\sigma(pp \to S \to jj) \times A \lesssim 12$ pb in ATLAS [39] and $\sigma(pp \to S \to gg) \times A \lesssim 1.8$ pb in CMS [34] for $m_S \approx 750\,\mathrm{GeV}$. For the CMS search, using parton level simulation we estimate the acceptance $A \approx 0.56$. The corresponding dijet cross section at the Tevatron is below a femtobarn, and therefore well below the sensitivity of the CDF search [40].

Two final remarks are in order here. One is that the results remain unchanged if the singlet scalar is replaced by a pseudo-scalar with the effective couplings [41]:

$$\mathcal{L} \supset \frac{e^2}{4v} \tilde{c}_{s\gamma\gamma} S F_{\mu\nu} \tilde{F}_{\mu\nu} + \frac{g_s^2}{4v} \tilde{c}_{sgg} S G_{\mu\nu}^a \tilde{G}_{\mu\nu}^a \,, \tag{3.7}$$
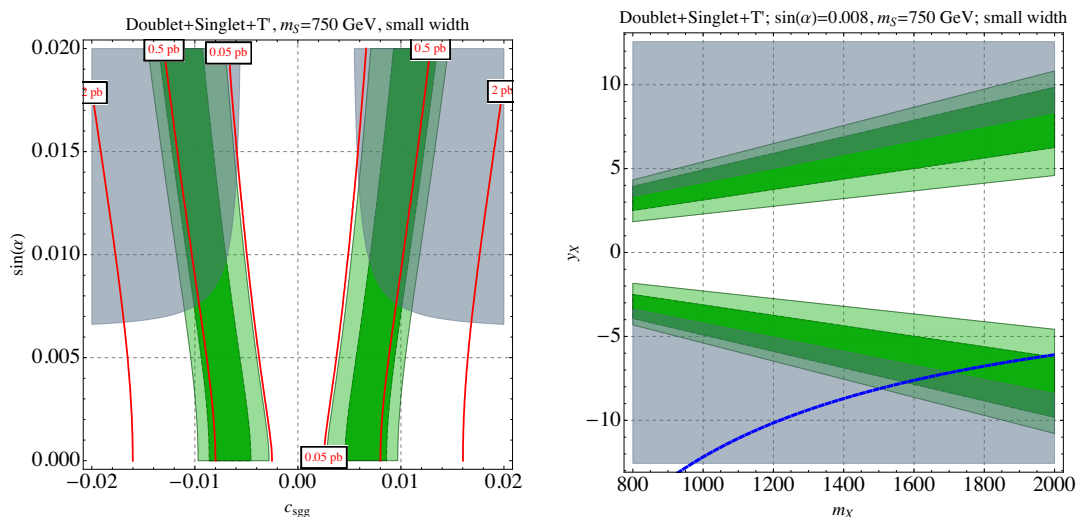
Figure 6. *Left:* the 68% CL (darker green) and 95% CL (lighter green) regions of the parameter space of the doublet-singlet model with the singlet coupled to a vector-like quark with charge $Q_X = 2/3$. The gray region is the parameter space disfavored at 95% CL by ATLAS [42, 43] and CMS [29] searches for a heavy Higgs boson decaying to WW and ZZ. We also show the contours of constant $\sigma(pp \to S)\text{Br}(S \to gg)$ cross section. *Right:* the same for the mixing angle fixed as $\sin\alpha = 0.008$ and presented in the space of Yukawa coupling y_X and mass m_X of the vector-like quark. The dashed blue line marks the parameters for which the vector-like quark cancels the quadratic divergent contribution to the Higgs mass from the SM top quark.

which can be generated by integrating out a vector-like quark with the Yukawa coupling $-y_X S \bar{X} \gamma_5 X$. Then the favored parameter space is still that in figure 5 with the replacement $c_{svv} \to \tilde{c}_{svv}$.

The other remark is that, generically, integrating out vector-like quarks at one loop yields effective couplings not only to photons and gluons but also to ZZ, $Z\gamma$, and WW [10, 19, 21]. For example, if the vector-like quark has quantum numbers $(3,1)_{Q_X}$ under the SM gauge group then one obtains

$$\mathcal{L}_{S,\text{eff}} \supset \frac{e^2}{4vc_\theta^2}c_{s\gamma\gamma}SB_{\mu\nu}B_{\mu\nu} = \frac{e^2}{4v}c_{s\gamma\gamma}S\left(A_{\mu\nu}A_{\mu\nu} - 2t_\theta A_{\mu\nu}Z_{\mu\nu} + t_\theta^2 Z_{\mu\nu}Z_{\mu\nu}\right), \qquad (3.8)$$

where t_θ are the tangent of the weak mixing angle. In this case $\text{Br}(S \to Z\gamma)/\text{Br}(S \to \gamma\gamma) \approx 2t_\theta^2 \approx 0.6$, $\text{Br}(S \to ZZ)/\text{Br}(S \to \gamma\gamma) \approx t_\theta^4 \approx 0.1$. On the other hand, if the vector-like quark has zero hypercharge and non-trivial weak SU(2) quantum numbers, then one predicts $\text{Br}(S \to Z\gamma)/\text{Br}(S \to \gamma\gamma) \approx 2t_\theta^{-2} \approx 7$, $\text{Br}(S \to ZZ)/\text{Br}(S \to \gamma\gamma) \approx t_\theta^{-4} \approx 13$, and $\text{Br}(S \to WW)/\text{Br}(S \to \gamma\gamma) \approx 2s_\theta^{-4} \approx 40$. Other patterns may arise when different quantum numbers are assumed, or when the vector-like quarks mix with the SM ones.

4   The doublet-singlet model

The singlet model can be extended in a straightforward way. A particularly motivated scenario is the one in which the scalar and the SM Higgs boson h mix. Such a mixing alters

the production and decay modes of both the singlet and doublet. Consequently, precision Higgs measurements and resonant searches in various channels (the most important one being $S \to WW$) place strong constraints on the available parameter space.

As before, we assume that the singlet couples to new vector-like quarks via the Yukawa coupling $\mathcal{L} \supset -y_X S\bar{X}X$. In addition, we assume that it couples to the SM via the Higgs portal, that is through the coupling $S|H|^2$. Then, after electroweak symmetry breaking, the mass matrix of the scalars contains off-diagonal terms. To diagonalize the mass matrix one needs to perform the rotation,

$$h \to h \cos\alpha + S \sin\alpha, \qquad S \to -h\sin\alpha + S\cos\alpha, \qquad (4.1)$$

where h is the physical Higgs mode. From the Higgs coupling measurements, the mixing angle is constrained at 95% CL to be, $\sin\alpha \lesssim 0.4$ [44], independently of m_S. Electroweak precision tests impose slightly stronger constraints in the relevant mass range: following the analysis of ref. [45], for a $m_S = 750\,\text{GeV}$ one finds $\sin\alpha \leq 0.32$ at 95% CL. In what follows, we study further constraints on the mixing angle assuming S is responsible for the diphoton excess at $750\,\text{GeV}$. As in the toy model, we find that the decay width of S is always narrow in the relevant parameter space, and therefore the analysis using the narrow width approximation is adequate.

Due to the mixing, the singlet acquires direct couplings to the SM gauge bosons and fermions,

$$\mathcal{L} \supset \frac{1}{v} \left(h \cos\alpha + S \sin\alpha \right) \left[2m_W^2 W_\mu^+ W_\mu^- + m_Z^2 Z_\mu Z_\mu - \sum_f m_f \bar{f}f \right]. \qquad (4.2)$$

This opens the possibility for S to decay to a pair of on-shell W and Z bosons. At the same time, the tree-level Higgs couplings to the SM matter is reduced by $\cos\alpha$, while the one-loop couplings to gluons and photons may be altered. Furthermore, integrating out the vector-like quark, induces the effective couplings of both S and h to gluons and photons:

$$\mathcal{L} \supset \frac{e^2}{4v} c_{s\gamma\gamma} \cos\alpha \, S F_{\mu\nu} F_{\mu\nu} + \frac{g_s^2}{4v} c_{sgg} \cos\alpha \, S G_{\mu\nu}^a G_{\mu\nu}^a$$
$$- \frac{e^2}{4v} c_{s\gamma\gamma} \sin\alpha \, h F_{\mu\nu} F_{\mu\nu} - \frac{g_s^2}{4v} c_{sgg} \sin\alpha \, h G_{\mu\nu}^a G_{\mu\nu}^a \qquad (4.3)$$

where c_{svv} are given in eq. (3.3). As in the toy model, the couplings in the first line allow S to be produced at the LHC and to decay to photons. The couplings in the second line, together with the modifications in eq. (4.2), affect the Higgs production cross-sections and decay widths. We apply the experimental constraints on these couplings from LHC Higgs searches using the likelihood function derived in ref. [46].

In figure 6 we show the results assuming that the vector-like quark X has charge $Q_X = 2/3$, that is to say, it is a T' quark with the same color and electromagnetic quantum numbers as the SM top quark. We can see that, in this case, the searches for heavy scalars in the diboson decay channel place stringent limits on the mixing angle in the parameters space favored by the diphoton excess, $\sin\alpha \lesssim 0.01$. The impact of the Higgs coupling measurements is weaker in the T' case.
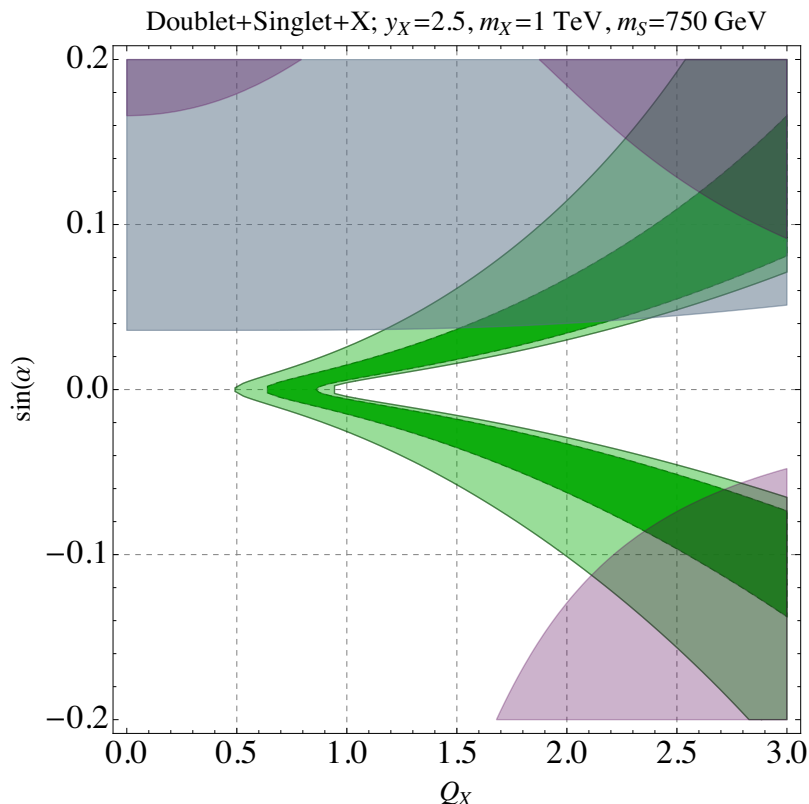
Figure 7. The 68% CL (darker green) and 95% CL (lighter green) regions of the parameter space of the doublet-singlet model in the $\sin\alpha$-Q_X plane, for a fixed Yukawa coupling $y_X = 2.5$ and $m_X = 1\,\mathrm{TeV}$, which corresponds to $c_{sgg} \approx 0.005$. The gray-shaded region is the parameter space disfavored at 95% CL by ATLAS [42, 43] and CMS [29] searches for a heavy Higgs boson decaying to WW and ZZ. The purple-shaded region is disfavored at 95% CL by Higgs couplings measurements [46]. The asymmetry of these two regions between positive and negative $\sin\alpha$ is due to interference between the SM and X contributions to the effective S and h coupling to gluons and photons.

Changing Q_X or choosing a more complicated pattern of the vector-like quarks, we can change the relation between c_{sgg} and $c_{s\gamma\gamma}$ compared to the T' case. This opens up more of the parameter space and allows for larger values of the mixing angle, as shown in figure 7 and figure 8. We find that the mixing angles as large as $\sin\alpha = 0.1$ can be accommodated in this framework, for sufficiently large Yukawa coupling, y_X. For larger $\sin\alpha$ the Higgs couplings measurements (especially the $h \to \gamma\gamma$ rate) exclude the entire parameter space fitting the 750 GeV excess and still allowed by diboson resonance searches. We also note that in the model with $c_{sgg} = 0$, that is when X is a vector-like lepton with no color charge, there is no allowed parameter space at all that fits the 750 GeV excess.

5 A broad resonance?

As can be seen in figure 4, the LHC diphoton data allow for a fairly wide $\mathcal{O}(10)$-$\mathcal{O}(100)$ GeV resonance at 750 GeV, which is significantly larger than the experimental resolution. While
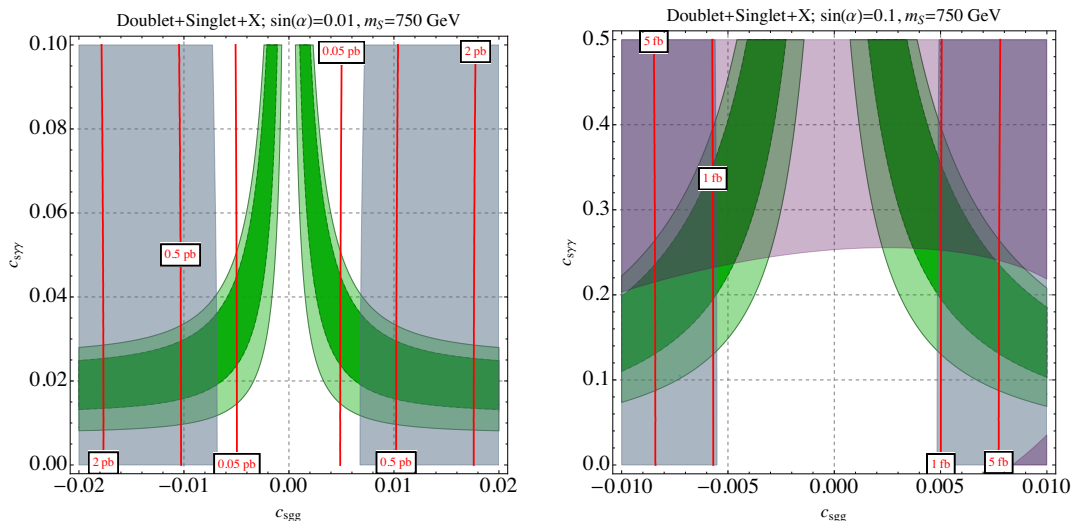
Figure 8. The 68% CL (darker green) and 95% CL (lighter green) regions of the parameter space of the doublet-singlet model in the c_{sgg}-$c_{s\gamma\gamma}$ plane, for a fixed value of the mixing angle $\sin\alpha = 0.01$ (*left*) and $\sin\alpha = 0.1$ (*right*). The red lines are contours of constant $\sigma(pp \rightarrow gg)$ cross section at $\sqrt{s} = 13\,\text{TeV}$ LHC. The gray-shaded region is the parameter space disfavored at 95% CL by ATLAS [42, 43] and CMS [29] searches for a heavy Higgs boson decaying to WW and ZZ. The purple-shaded region is disfavored at 95% CL by Higgs couplings measurements [46].

these hints are not statistically significant at this point, it is interesting to contemplate on the implications of such a possibility within the context of the singlet scenario.

We argue that, for the scalar singlet model considered here, and in the absence of additional degrees of freedom that couple to S, the width is always narrow in the relevant parameter space, even if the singlet mixes with the Higgs boson. Evidence for a wide resonance would therefore hint towards models with a light hidden sector to which the 750 GeV particle could decay with a sizable branching fraction. This sector may or may not be strongly coupled and identifying accompanying experimental signatures may clarify the situation. We distinguish between two distinct possibilities for the origin of the large width:

1. S decays invisibly into the hidden sector.

2. S decays into visible matter, possibly via cascade decays that may or may not involve hidden sector intermediate states.

In the case (1) the most significant signature is a monojet signal discussed in the next section. As we will argue then, this possibility is difficult to realize, given the existing experimental constraints. Conversely, case (2) predicts additional visible channels which must accompany the diphoton signal. If a broad resonance is confirmed, such model-dependent visible channels must exist, unless several semi-degenerate states hide underneath the observed 750 GeV resonance.

Irrespective of what the final state is, a larger width typically implies smaller branching fraction into diphotons. Therefore, the production cross-section must grow as one dials up the total width, in order to fit the LHC excess. Consequently, the rate of exotic processes of
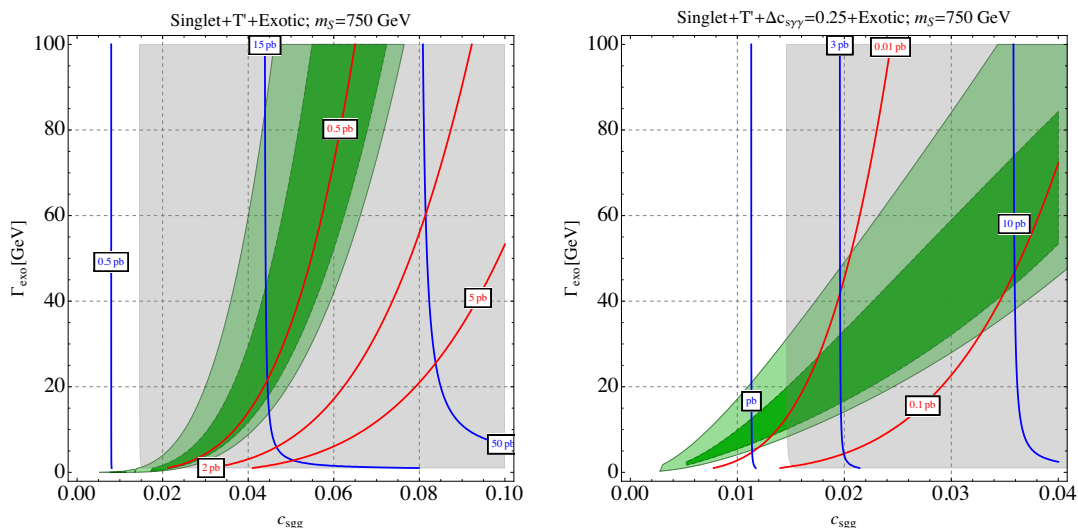
Figure 9. *Left:* best-fit region for a 750 GeV resonance with a varying width as a function of c_{sgg}, assuming a T' vector-like model. Red (blue) lines are the contours of constant digluon (exotic) cross section at the LHC with $\sqrt{s} = 13$ TeV. The gray-shaded area is excluded at 95% CL by ATLAS [47] and CMS [48] monojet searches at $\sqrt{s} = 8$ TeV, assuming the exotic width corresponds to S decays to invisible particles. *Right:* the same when, in addition to a T', the model predicts another contribution to the effective coupling of the singlet to photons, $\Delta c_{s\gamma\gamma} = 0.25$.

the type (1) or (2) also increases in the interesting parameter space. In the left panel of figure 9 we demonstrate this effect, by plotting the best-fit region for a 750 GeV resonance with a varying exotic width Γ_{exo} as a function of the singlet-gluon-gluon couplings, c_{egg}, assuming a T' vector-like model. The electric charge of T' sets the gluon-gluon to gamma-gamma ratio, as in eq. (3.3). The red and blue contours indicate, respectively, the predicted di-gluon and exotic cross sections in the $\sqrt{s} = 13$ TeV LHC . Note that the exotic cross section could also be just dijet, if e.g. the large width is due to large singlet coupling to heavier SM quarks. One can see that, in this case, a large width, $\Gamma \gtrsim 20$ GeV, implies an exotic cross section of at least $O(10)$ pb in the parameter space relevant for the 750 GeV excess. In the plot we assume no mixing of the singlet with the Higgs boson, however similar conclusions are reached when mixing is allowed. The conclusion can be changed if the ratio between the γ-γ and gluon-gluon effective couplings is larger than that predicted by the singlet model with T'. In the right panel of figure 9 we show the situation in a model where, in addition to a T', there are new vector-like leptons providing a very large contribution to the effective coupling of the singlet to photons. As a reference, $\Delta c_{s\gamma\gamma} = 0.25$ corresponds e.g. to 15 vector-like leptons (τ') with $m_{\tau'} = 750$ GeV and a Yukawa coupling to the singlet, $y_{\tau'} = 3$. Nevertheless, even in such an artificially doped scenario, an exotic cross section at least at the picobarn level is predicted in the favored parameter space with a large width. We thus conclude that a search for invisible or exotic signals in run-2 could allow for a spectacular confirmation of the 750 GeV excess and provide precious new information for model builders.

6 Experimental consequences

A statistical confirmation of the excess in the diphoton signal will require the collection of additional data. Meanwhile, several other channels provide additional constraints and may shed light on the possible nature of the resonance. Indeed, $\mathcal{O}(1)$ diphoton branching fractions are unusual for scalar particles once other channels are kinematically available. Even for the 125 GeV Higgs boson, BR($h \to \gamma\gamma$) is only 0.2%, while for a would-be 750 GeV SM Higgs boson one has BR($h \to \gamma\gamma$) $\sim 10^{-7}$ [36]. Therefore, it is highly probable that the new particle has other decay channels. Below we briefly comment on some existing constraints and possible signals.

- **Dijets.** As illustrated in figures 5, 6, 8 and 9, the dijet rate can be significant in the interesting parameter space. This is a general conclusion for scenarios where the 750 GeV resonance is produced in gluon-gluon collisions. It is therefore crucial to attempt dijet resonance searches in the 700-800 GeV ballpark. In the minimal toy model, dijet cross-sections of order 1-10 picobarns in the $\sqrt{s} = 13$ TeV LHC can be easily achieved, see figure 5. This conclusion also holds for a large resonance width, see figure 9. Once the singlet mixes significantly with the Higgs boson, constraints from diboson channels preclude a large digluon cross section.

    Current limits from dijet resonance searches at $\sqrt{s} = 8$ TeV ATLAS [39] and CMS [34] read, respectively, $\sigma(pp \to gg) \times A \leq 11$ pb and $\sigma(pp \to gg) \times A \leq 1.8$ pb at 750 GeV. Using simulations in Madgraph we estimate the efficiency times acceptance of the CMS search as $A \approx 0.56$. The resulting limit does not constrain the available parameter space, except for the large c_{sgg} region in the pure-singlet scenario (see figure 5). We expect upcoming trigger-level dijet analysis to improve the limits, possibly allowing to detect the predicted signal in this mass range.

- **Dibosons.** If the scalar mixes with the SM Higgs boson, generically a large signal in the WW and ZZ channels is predicted. As discussed earlier, the ATLAS and CMS heavy Higgs searches in the WW channel in run-1 result in a strong constraint on the mixing angle, $\sin\alpha \lesssim 0.1$. Future improvements of the sensitivity in run-2 will further constrain the parameter space of the model or reveal a signal. More generally, in models where scalar decays to $\gamma\gamma$ arise due to loops of heavy particles, decays to WW, ZZ, and $Z\gamma$ typically occur with rates comparable to the diphoton one. For example, if the particle dominating the loop is charged under the SM $U(1)_Y$ and an $SU(2)_L$ singlet, then one predicts $\mathrm{Br}(S \to Z\gamma) \simeq 0.6\mathrm{Br}(S \to \gamma\gamma)$. Given the diphoton cross section fitting the LHC data, see figure 3, the cross section in the $Z\gamma$ channel is predicted to be $\sim$ 1-2 fb in the $\sqrt{s} = 13$ TeV LHC, and $\sim$ 0.2-0.4 fb at $\sqrt{s} = 8$ TeV. The run-1 ATLAS resonance search in the $Z\gamma$ channel excludes $\sigma(pp \to S)\mathrm{Br}(S \to Z\gamma) \gtrsim 4$ fb in the fiducial volume [49], which is only an order of magnitude above the predicted signal. On the other hand, if the particle dominating the loop is charged under the SM $SU(2)_L$ and a singlet of $U(1)_Y$, one predicts $\mathrm{Br}(S \to Z\gamma) \simeq 7\mathrm{Br}(S \to \gamma\gamma)$, and then the cross section in the $Z\gamma$ channel is predicted to be of order 1-6 fb at $\sqrt{s} = 8$ TeV. As shown in figure 10, this already limits the available
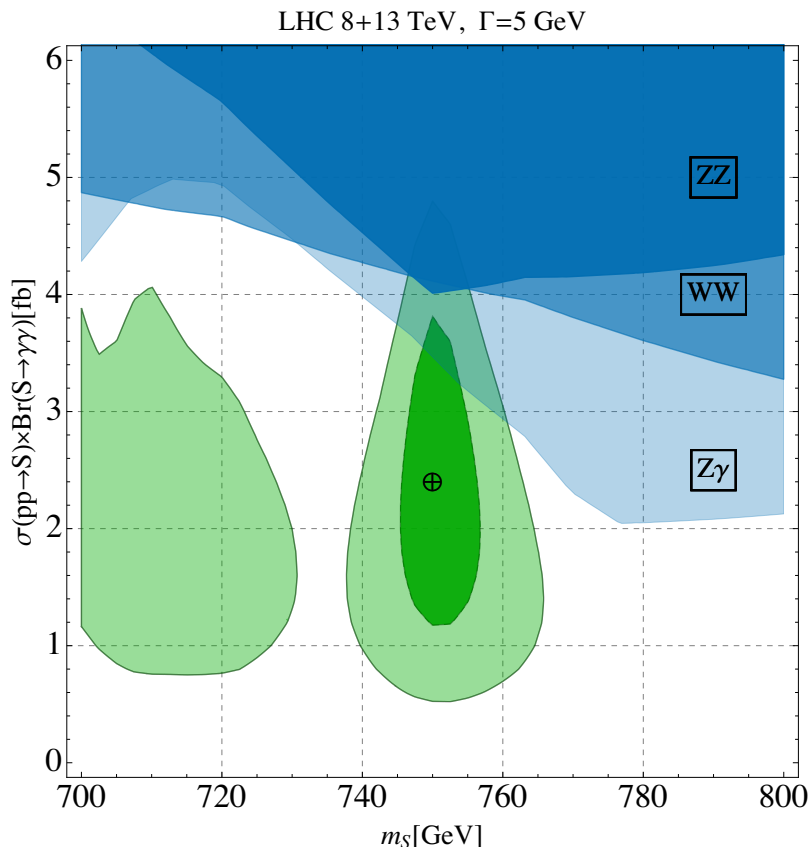
Figure 10. The same as figure 3 (left) but with overlaid limits from ATLAS $Z\gamma$ [49], WW [42], and ZZ [43] resonance searches (different shades of blue) at $\sqrt{s} = 8\,\mathrm{TeV}$, assuming the particle generating the effective coupling of the singlet to photons and gluons has zero hypercharge. For the $Z\gamma$ limits, we took the acceptance in the fiducial volume $A \approx 0.7$ for $m_S \approx 750\,\mathrm{GeV}$, estimated using Madgraph simulations of the $pp \to S \to (Z \to \ell^+\ell^-)\gamma$ process.

parameter space, putting the constraint $\sigma \lesssim 3.5\,\mathrm{fb}$ on the diphoton cross section at $\sqrt{s} = 13\,\mathrm{TeV}$ for $m_S \approx 750\,\mathrm{GeV}$. Furthermore, for this kind particle in the loop, the limits from the WW and ZZ channels [42, 43] are only a factor of 2 weaker.

- **New colored states.** New particles (fermions or bosons) with a color and electric charge and a large coupling to the 750 GeV singlet scalar are needed to generate an effective coupling of the scalar to gluons and photons. These new colored states should not be too heavy, otherwise their couplings to the scalar must enter the non-perturbative regime in order to explain the diphoton excess. As can be seen in figure 8, in a model where a new vector-like top quark is the only new colored state, its Yukawa couplings to the scalar must already be $y_{T'} \gtrsim 3$ for $m_{T'} \approx 1\,\mathrm{TeV}$. Therefore, if this interpretation of the diphoton excess is correct, one expects new colored states just around the corner. These new states may decay to the SM (if they mix with the SM matter) or they can be stable on the collider scale in which case the search for heavy stable states and R-hadrons become important.

- **Monojets.** Following the discussion in the previous section, it is a priori possible to explain a broad resonance through decays of the scalar to invisible particles, $S \to \chi\chi$. In figure 9, the blue contours should then be interpreted as an invisible cross section, $\sigma(pp \to \chi\chi)$ at $\sqrt{s} = 13\,\text{TeV}$. That is not directly observable in a collider, however the associated monojet signature can be observed, when the invisible particles recoil against an energetic jet emitted in the process. Limits on this scenario may be derived from run-1 monojet searches in ATLAS [47] and CMS [48] which put constraints on the monojet rates with $p_{T,\text{miss}}$ ranging from 150 to 700 GeV. As an example, the monojet cross section, $\sigma(pp \to \chi\chi g)$ with $p_{T,\text{miss}} > 500\,\text{GeV}$ at $\sqrt{s} = 8\,\text{TeV}$, calculated at the leading order using Madgraph, is a factor 3×10^{-3} smaller than the invisible cross section. For this missing energy bin, the ATLAS (CMS) quote the constraint $\sigma \lesssim 7(6)\,\text{fb}$. On the other hand, in the best-fit region of the T' model where the resonance is broad one predicts the monojet rate well above $10\,\text{fb}$, which is excluded (cf. the gray-shaded region in the left panel of figure 9.) We thus conclude that it is problematic to address the broadness of the resonance by assuming a large invisible width. Instead, if the hints of $\mathcal{O}(10 - 100)\,\text{GeV}$ width are confirmed, new visible (though possibly exotic) signals would be expected to accompany the diphoton signal. This conclusion can be circumvented if a new large contribution to the effective coupling to photons is present, as in the right panel of figure 9. However, huge contributions are required to this end, possibly pointing to UV completions by a large N_c strongly interacting theory [19].

- **Hidden valley and lepton jets.** Given the strong constraint from monojets on the invisible decay width, it is possible that S cascades to additional hidden-sector particles which then, at least in part, decay visibly. This scenario is referred to as the *hidden valley* models [8] and their precise signature is strongly model-dependent. Here we mention one interesting possibility of decays to lepton jets [50], which can be e.g. realized in a similar model as in ref. [51]. Such decays may occur promptly or induce displaced vertices, depending on the corresponding parameter space. Limits on such a scenario have been studied mostly for a light scalar and cannot be straightforwardly interpreted for this scenario (see e.g. [52–58]). Additional searches are thus required and may place interesting (even if model-dependent) limits.

7 Outlook: naturalness around the corner?

In this paper we argued that the SM supplemented by a 750 GeV singlet scalar and an $\mathcal{O}(1)\,\text{TeV}$ vector-like quark with a sizable Yukawa coupling to the singlet can very well explain the observed 750 GeV diphoton excess. This explanation continues to be valid if the singlet has a small mixing $\sin\alpha \lesssim 0.1$ with the SM Higgs boson. While a broad-width resonance fits the data better, a narrow resonance is still consistent with the present data. Given the strong available monojet constraints, if a broad resonance is confirmed it is challenging to explain with a sizable invisible width. Consequently, accompanying model-dependent visible channels are expected, unless underneath the resonance lie a set

of degenerate states. In addition, we find that upcoming dijet searches will allow for an exciting model-independent confirmation of the singlet interpretation to the data.

From the purely phenomenological view point, it is possible that this simple extension constitutes the complete theory of fundamental interactions at the TeV scale. Nevertheless, a reasonable expectation is that these degrees of freedom are just a tip of an iceberg, revealing the hints of a more sophisticated structure of physics beyond the SM. An exciting possibility is that this larger structure is responsible for solving the hierarchy problem of the SM.

The diphoton excess may hint to such a possibility. Indeed, if the resonance couples to photons and gluons via one-loop diagrams, it must couple to colored and electrically charged particles. Such states may then be involved in canceling the top-induced quadratically divergent contribution to the Higgs mass. In the case of a mixing between the singlet and Higgs doublet, such colored states couple to the Higgs and may result in the desired cancelation. It is therefore interesting to ask whether such a cancelation occurs in the allowed parameter space. The blue line in figure 6 shows the parameters in the singlet-fermion Yukawa coupling vs. fermion mass plane where such a cancelation occurs. Interestingly, this possibility is not excluded and implies that the observed resonance may be a first hint of naturalness. Closing in on this region and identifying the accompanying channels may therefore enable us to progress towards a solution to the naturalness problem.

Acknowledgments

References

[1] ATLAS collaboration, *Search for resonances decaying to photon pairs in* $3.2\,\mathrm{fb}^{-1}$ *of pp collisions at* $\sqrt{s} = 13\,TeV$ *with the ATLAS detector*, ATLAS-CONF-2015-081, CERN, Geneva Switzerland (2015).

[2] CMS collaboration, *Search for new physics in high mass diphoton events in proton-proton collisions at* $\sqrt{s} = 13\,TeV$, CMS-PAS-EXO-15-004, CERN, Geneva Switzerland (2015).

[3] L.D. Landau, *On the angular momentum of a system of two photons*, *Dokl. Akad. Nauk Ser. Fiz.* **60** (1948) 207 [InSPIRE].

[4] C.-N. Yang, *Selection rules for the dematerialization of a particle into two photons*, *Phys. Rev.* **77** (1950) 242 [InSPIRE].

[5] Z. Chacko, H.-S. Goh and R. Harnik, *The twin Higgs: natural electroweak breaking from mirror symmetry*, *Phys. Rev. Lett.* **96** (2006) 231802 [hep-ph/0506256] [INSPIRE].

[6] L. Randall and R. Sundrum, *A large mass hierarchy from a small extra dimension*, *Phys. Rev. Lett.* **83** (1999) 3370 [hep-ph/9905221] [INSPIRE].

[7] V. Silveira and A. Zee, *Scalar phantoms*, *Phys. Lett.* **B 161** (1985) 136 [INSPIRE].

[8] M.J. Strassler and K.M. Zurek, *Echoes of a hidden valley at hadron colliders*, *Phys. Lett.* **B 651** (2007) 374 [hep-ph/0604261] [INSPIRE].

[9] D. Carmi, A. Falkowski, E. Kuflik, T. Volansky and J. Zupan, *Higgs after the discovery: a status report*, *JHEP* **10** (2012) 196 [arXiv:1207.1718] [INSPIRE].

[10] T. Higaki, K.S. Jeong, N. Kitajima and F. Takahashi, *The QCD axion from aligned axions and diphoton excess*, *Phys. Lett.* **B 755** (2016) 13 [arXiv:1512.05295] [INSPIRE].

[11] S.D. McDermott, P. Meade and H. Ramani, *Singlet scalar resonances and the diphoton excess*, arXiv:1512.05326 [INSPIRE].

[12] M. Low, A. Tesi and L.-T. Wang, *A pseudoscalar decaying to photon pairs in the early LHC run 2 data*, arXiv:1512.05328 [INSPIRE].

[13] B. Bellazzini, R. Franceschini, F. Sala and J. Serra, *Goldstones in diphotons*, arXiv:1512.05330 [INSPIRE].

[14] C. Petersson and R. Torre, *The 750 GeV diphoton excess from the goldstino superpartner*, arXiv:1512.05333 [INSPIRE].

[15] E. Molinaro, F. Sannino and N. Vignaroli, *Strong dynamics or axion origin of the diphoton excess*, arXiv:1512.05334 [INSPIRE].

[16] J. Ellis, S.A.R. Ellis, J. Quevillon, V. Sanz and T. You, *On the interpretation of a possible ∼ 750 GeV particle decaying into γγ*, arXiv:1512.05327 [INSPIRE].

[17] R.S. Gupta, S. Jäger, Y. Kats, G. Perez and E. Stamou, *Interpreting a 750 GeV diphoton resonance*, arXiv:1512.05332 [INSPIRE].

[18] S. Di Chiara, L. Marzola and M. Raidal, *First interpretation of the 750 GeV di-photon resonance at the LHC*, arXiv:1512.04939 [INSPIRE].

[19] R. Franceschini et al., *What is the γγ resonance at 750 GeV?*, arXiv:1512.04933 [INSPIRE].

[20] A. Pilaftsis, *Diphoton signatures from heavy axion decays at the CERN Large Hadron Collider*, *Phys. Rev.* **D 93** (2016) 015017 [arXiv:1512.04931] [INSPIRE].

[21] D. Buttazzo, A. Greljo and D. Marzocca, *Knocking on new physics' door with a scalar resonance*, arXiv:1512.04929 [INSPIRE].

[22] S. Knapen, T. Melia, M. Papucci and K. Zurek, *Rays of light from the LHC*, arXiv:1512.04928 [INSPIRE].

[23] Y. Nakai, R. Sato and K. Tobioka, *Footprints of new strong dynamics via anomaly*, arXiv:1512.04924 [INSPIRE].

[24] A. Angelescu, A. Djouadi and G. Moreau, *Scenarii for interpretations of the LHC diphoton excess: two Higgs doublets and vector-like quarks and leptons*, arXiv:1512.04921 [INSPIRE].

[25] M. Backovic, A. Mariotti and D. Redigolo, *Di-photon excess illuminates dark matter*, arXiv:1512.04917 [INSPIRE].

[26] Y. Mambrini, G. Arcadi and A. Djouadi, *The LHC diphoton resonance and dark matter*, arXiv:1512.04913 [INSPIRE].

[27] K. Harigaya and Y. Nomura, *Composite models for the* 750 *GeV diphoton excess*, *Phys. Lett.* **B 754** (2016) 151 arXiv:1512.04850 [INSPIRE].

[28] ATLAS collaboration, *Search for high-mass diphoton resonances in pp collisions at* $\sqrt{s} = 8\,TeV$ *with the ATLAS detector*, *Phys. Rev.* **D 92** (2015) 032004 arXiv:1504.05511 [INSPIRE].

[29] CMS collaboration, *Search for diphoton resonances in the mass range from* 150 *to* 850 *GeV in pp collisions at* $\sqrt{s} = 8\,TeV$, *Phys. Lett.* **B 750** (2015) 494 arXiv:1506.02301 [INSPIRE].

[30] D. Carmi, A. Falkowski, E. Kuflik and T. Volansky, *Interpreting LHC Higgs results from natural new physics perspective*, *JHEP* **07** (2012) 136 arXiv:1202.3144 [INSPIRE].

[31] G. Moreau, *Constraining extra-fermion(s) from the Higgs boson data*, *Phys. Rev.* **D 87** (2013) 015027 arXiv:1210.3977 [INSPIRE].

[32] M.-L. Xiao and J.-H. Yu, *Stabilizing electroweak vacuum in a vectorlike fermion model*, *Phys. Rev.* **D 90** (2014) 014007 [*Addendum ibid.* **D 90** (2014) 019901] arXiv:1404.0681 [INSPIRE].

[33] D. Karabacak, S. Nandi and S.K. Rai, *New signal for singlet Higgs and vector-like quarks at the LHC*, *Phys. Lett.* **B 737** (2014) 341 arXiv:1405.0476 [INSPIRE].

[34] CMS collaboration, *Search for resonances decaying to dijet final states at* $\sqrt{s} = 8\,TeV$ *with scouting data*, [CMS-PAS-EXO-14-005](CMS-PAS-EXO-14-005), CERN, Geneva Switzerland (2014).

[35] A.D. Martin, W.J. Stirling, R.S. Thorne and G. Watt, *Parton distributions for the LHC*, *Eur. Phys. J.* **C 63** (2009) 189 arXiv:0901.0002 [INSPIRE].

[36] LHC HIGGS CROSS SECTION WORKING GROUP collaboration, J.R. Andersen et al., *Handbook of LHC Higgs cross sections: 3. Higgs properties*, arXiv:1307.1347 [INSPIRE].

[37] ATLAS collaboration, *Search for new phenomena in dijet mass and angular distributions from pp collisions at* $\sqrt{s} = 13\,TeV$ *with the ATLAS detector*, *Phys. Lett.* **B 754** (2016) 302 arXiv:1512.01530 [INSPIRE].

[38] CMS collaboration, *Search for narrow resonances decaying to dijets in proton-proton collisions at* $\sqrt{s} = 13\,TeV$, arXiv:1512.01224 [INSPIRE].

[39] ATLAS collaboration, *Search for new phenomena in the dijet mass distribution using pp collision data at* $\sqrt{s} = 8\,TeV$ *with the ATLAS detector*, *Phys. Rev.* **D 91** (2015) 052007 arXiv:1407.1376 [INSPIRE].

[40] CDF collaboration, T. Aaltonen et al., *Search for new particles decaying into dijets in proton-antiproton collisions at* $\sqrt{s} = 1.96\,TeV$, *Phys. Rev.* **D 79** (2009) 112002 arXiv:0812.4036 [INSPIRE].

[41] J. Jaeckel, M. Jankowiak and M. Spannowsky, *LHC probes the hidden sector*, *Phys. Dark Univ.* **2** (2013) 111 arXiv:1212.3620 [INSPIRE].

[42] ATLAS collaboration, *Search for a high-mass Higgs boson decaying to a W boson pair in pp collisions at* $\sqrt{s} = 8\,TeV$ *with the ATLAS detector*, *JHEP* **01** (2016) 032 arXiv:1509.00389 [INSPIRE].

[43] ATLAS collaboration, *Search for an additional, heavy Higgs boson in the $H \to ZZ$ decay channel at $\sqrt{s} = 8\,TeV$ in pp collision data with the ATLAS detector*, *Eur. Phys. J.* **C 76** (2016) 45 [arXiv:1507.05930] [inSPIRE].

[44] ATLAS and CMS collaborations, *Measurements of the Higgs boson production and decay rates and constraints on its couplings from a combined ATLAS and CMS analysis of the LHC pp collision data at $\sqrt{s} = 7$ and $8\,TeV$*, ATLAS-CONF-2015-044, CERN, Geneva Switzerland (2015).

[45] A. Falkowski, C. Gross and O. Lebedev, *A second Higgs from the Higgs portal*, *JHEP* **05** (2015) 057 [arXiv:1502.01361] [inSPIRE].

[46] A. Falkowski, *Effective field theory approach to LHC Higgs data*, arXiv:1505.00046 [inSPIRE].

[47] ATLAS collaboration, *Search for new phenomena in final states with an energetic jet and large missing transverse momentum in pp collisions at $\sqrt{s} = 8\,TeV$ with the ATLAS detector*, *Eur. Phys. J.* **C 75** (2015) 299 [*Erratum ibid.* **C 75** (2015) 408] [arXiv:1502.01518] [inSPIRE].

[48] CMS collaboration, *Search for dark matter, extra dimensions and unparticles in monojet events in proton-proton collisions at $\sqrt{s} = 8\,TeV$*, *Eur. Phys. J.* **C 75** (2015) 235 [arXiv:1408.3583] [inSPIRE].

[49] ATLAS collaboration, *Search for new resonances in $W\gamma$ and $Z\gamma$ final states in pp collisions at $\sqrt{s} = 8\,TeV$ with the ATLAS detector*, *Phys. Lett.* **B 738** (2014) 428 [arXiv:1407.8150] [inSPIRE].

[50] N. Arkani-Hamed and N. Weiner, *LHC signals for a superunified theory of dark matter*, *JHEP* **12** (2008) 104 [arXiv:0810.0714] [inSPIRE].

[51] A. Falkowski, J.T. Ruderman, T. Volansky and J. Zupan, *Discovering Higgs decays to lepton jets at hadron colliders*, *Phys. Rev. Lett.* **105** (2010) 241801 [arXiv:1007.3496] [inSPIRE].

[52] ATLAS collaboration, *Search for long-lived neutral particles decaying into lepton jets in proton-proton collisions at $\sqrt{s} = 8\,TeV$ with the ATLAS detector*, *JHEP* **11** (2014) 088 [arXiv:1409.0746] [inSPIRE].

[53] ATLAS collaboration, *Search for WH production with a light Higgs boson decaying to prompt electron-jets in proton-proton collisions at $\sqrt{s} = 7\,TeV$ with the ATLAS detector*, *New J. Phys.* **15** (2013) 043009 [arXiv:1302.4403] [inSPIRE].

[54] ATLAS collaboration, *Search for displaced muonic lepton jets from light Higgs boson decay in proton-proton collisions at $\sqrt{s} = 7\,TeV$ with the ATLAS detector*, *Phys. Lett.* **B 721** (2013) 32 [arXiv:1210.0435] [inSPIRE].

[55] ATLAS collaboration, *Search for pair produced long-lived neutral particles decaying in the ATLAS hadronic calorimeter in pp collisions at $\sqrt{s} = 8\,TeV$*, ATLAS-CONF-2014-041, CERN, Geneva Switzerland (2014).

[56] CMS collaboration, *A search for pair production of new light bosons decaying into muons*, *Phys. Lett.* **B 752** (2016) 146 [arXiv:1506.00424] [inSPIRE].

[57] ATLAS collaboration, *A search for prompt lepton-jets in pp collisions at $\sqrt{s} = 8\,TeV$ with the ATLAS detector*, *JHEP* **02** (2016) 062 [arXiv:1511.05542] [inSPIRE].

[58] ATLAS collaboration, *A search for prompt lepton-jets in pp collisions at $\sqrt{s} = 7\,TeV$ with the ATLAS detector*, *Phys. Lett.* **B 719** (2013) 299 [arXiv:1212.5409] [inSPIRE].